Bone Reports 20 (2024) 101735

Contents lists available at ScienceDirect

Bone Reports

journal homepage: www.elsevier.com/locate/bonr

Am I big boned? Bone length scaled reference data for HRpQCT measures of the radial and tibial diaphysis in White adults

Stuart J. Warden [a,b,*], Robyn K. Fuchs [b,c], Ziyue Liu [b,d], Katelynn R. Toloday [a], Rachel Surowiec [e], Sharon M. Moe [b,f]

[a] Department of Physical Therapy, School of Health and Human Sciences, Indiana University, Indianapolis, IN, United States of America
[b] Indiana Center for Musculoskeletal Health, Indiana University, IN, United States of America
[c] College of Osteopathic Medicine, Marian University, Indianapolis, IN, United States of America
[d] Department of Biostatistics, School of Medicine, Indiana University, Indianapolis, IN, United States of America
[e] Department of Biomedical Engineering, Purdue University, Indianapolis, IN, United States of America
[f] Division of Nephrology and Hypertension, Department of Medicine, School of Medicine, Indiana University, Indianapolis, IN, United States of America

ARTICLE INFO

Keywords:
Bone allometry
Bone strength
Cortical bone
Normative data
Osteoporosis

ABSTRACT

Cross-sectional size of a long bone shaft influences its mechanical properties. We recently used high-resolution peripheral quantitative computed tomography (HRpQCT) to create reference data for size measures of the radial and tibial diaphyses. However, data did not take into account the impact of bone length. Human bone exhibits relatively isometric allometry whereby cross-sectional area increases proportionally with bone length. The consequence is that taller than average individuals will generally have larger z-scores for bone size outcomes when length is not considered. The goal of the current work was to develop a means of determining whether an individual's cross-sectional bone size is suitable for their bone length. HRpQCT scans performed at 30 % of bone length proximal from the distal end of the radius and tibia were acquired from 1034 White females (age = 18.0 to 85.3 y) and 392 White males (age = 18.4 to 83.6 y). Positive relationships were confirmed between bone length and cross-sectional areas and estimated mechanical properties. Scaling factors were calculated and used to scale HRpQCT outcomes to bone length. Centile curves were generated for both raw and bone length scaled HRpQCT data using the LMS approach. Excel-based calculators are provided to facilitate calculation of z-scores for both raw and bone length scaled HRpQCT outcomes. The raw z-scores indicate the magnitude that an individual's HRpQCT outcomes differ relative to expected sex- and age-specific values, with the scaled z-scores also considering bone length. The latter enables it to be determined whether an individual or population of interest has normal sized bones for their length, which may have implications for injury risk. In addition to providing a means of expressing HRpQCT bone size outcomes relative to bone length, the current study also provides centile curves for outcomes previously without reference data, including tissue mineral density and moments of inertia.

1. Introduction

Bone strength is influenced by the amount and quality of material present in addition to how the material is distributed (Fuchs et al., 2019). The distribution of bone material is colloquially referred to as bone structure or size and is often assessed via cross-sectional bone images acquired using 3D imaging modalities such as computed tomography and magnetic resonance imaging. High-resolution peripheral quantitative computed tomography (HRpQCT) is a powerful imaging modality capable of providing non-invasive measures of bone cross-sectional properties, along with volumetric bone mineral density (vBMD) and micro-finite element (μFE) estimates of bone strength (Whittier et al., 2020).

HRpQCT is principally used to assess structure at sites rich in trabecular bone (e.g., distal radius), with outcomes predicting incident fracture (Mikolajewicz et al., 2020; Samelson et al., 2019) and revealing the effects of aging, disease, and intervention (Lespessailles et al., 2016). However, there is growing interest in assessing more proximal sites containing a higher proportion of cortical bone (Cheung et al., 2014; Hughes et al., 2018; Kazakia et al., 2014; O'Leary et al., 2021; Orwoll

* Corresponding author at: Department of Physical Therapy, School of Health and Human Sciences, Indiana University, 1140 W. Michigan St., CF-120, Indianapolis, IN 46202, United States of America.
E-mail address: stwarden@iu.edu (S.J. Warden).

https://doi.org/10.1016/j.bonr.2024.101735
Received 9 December 2023; Accepted 4 January 2024
Available online 6 January 2024

et al., 2022; Patsch et al., 2013; Warden et al., 2022a; Warden et al., 2021a). Most bone loss during aging occurs from within the cortical compartment (Zebaze et al., 2010), and assessment of cortical bone-rich diaphyseal sites may provide unique insight into bone changes occurring in disease states and with lifestyle and pharmaceutical interventions.

We recently used a second-generation HRpQCT scanner to create reference data for cortical bone outcomes obtained at 30 % of bone length proximal from the distal end of the radius and tibia (Warden et al., 2022b). The data can be used to calculate z-scores to indicate the number of standard deviations an individual's outcomes vary from age- and sex-matched median outcomes. However, the reference data did not take into account the impact of bone length on cross-sectional bone size.

There has long been a fascination with the relationship between bone length and cross-sectional size. Galileo (Galilei, 1638) predicted that bones in different sized animals would exhibit positive allometry. That is, he predicted bone size would increase to a relatively greater extent than length in order to maintain the same strength. More recently, skeletal allometry in mammals, including humans, has been reported to be more modest with the relationship between bone length and cross-sectional size being closer to isometric (Biewener, 2005; Ruff, 1984). Specifically, the bones of taller people are generally expanded versions of bones of people who are shorter, with bone cross-sectional area increasing proportionally as bone length increases. The net result is that taller-than-average individuals will generally have larger z-scores for bone size outcomes using currently available reference HRpQCT data, and vice versa for shorter individuals.

The goal of the current study was to develop a means of determining whether an individual's cross-sectional bone size is suitable not only for their age and sex, but also their bone length. The primary aims were to: 1) explore the relationship between bone length and HRpQCT measures of radial and tibial diaphysis size in adults and 2) generate bone length scaled age- and sex-specific reference data for the HRpQCT measures across adulthood. In doing so, the current study also aimed to provide centile curves for outcomes previously without reference data, including tissue mineral density and moments of inertia. The ultimate goal was to provide calculators to enable the computation of subject-specific percentiles and z-scores for both raw and bone length scaled HRpQCT outcomes.

2. Methods

2.1. Participants

HRpQCT scans were performed on 1856 adults (aged ≥18 years) between 12/2017 and 12/2022 within the Musculoskeletal Function, Imaging, and Tissue Resource Core (FIT Core) of the Indiana Center for Musculoskeletal Health's Clinical Research Center (Indianapolis, Indiana). Participants were recruited to the core by investigators seeking standardized musculoskeletal outcomes for their research subjects, as well as from the local community via self-referral. The FIT Core has Institutional Review Board approval from Indiana University to assess all-comers who provide written informed consent.

To be eligible for inclusion in the current dataset, participants were required to: 1) self-identify as being of White ancestry, 2) be ambulatory and 3) have no self-reported diabetes, liver or kidney disease, past or present history of cancer, thyroid disorders, cystic fibrosis, or rare bone disease (e.g., osteopetrosis or X-linked hypophosphatemia). Individuals with the later conditions were excluded due to their overrepresentation in the FIT Core cohort resulting from investigator-initiated trials and their known or potential impact on HRpQCT outcomes (van den Bergh et al., 2021).

Height (m) and weight (kg) were measured without shoes using a calibrated stadiometer (Seca 264; Seca GmbH & Co., Hamburg, Germany) and scale (MS140-300; Brecknell, Fairmont, MN), respectively. Grip strength using a JamarPlus+ digital hand dynamometer (Sammons Preston, Bolingbrook, IL) and time to complete five sit-to-stand maneuvers without arms from standardized chair (seat height = 45 cm) were performed to assess physical function, as we have previously detailed (Warden et al., 2022c). Self-reported physical function was assessed using the physical functioning domain of the National Institutes of Health Patient Reported Outcomes Measurement Information System (PROMIS-PF), performed via computerized adaptive testing. PROMIS scores are standardized and expressed as T-scores with a population mean of 50 and standard deviation of 10 (Cella et al., 2007). Spine and total hip aBMD were assessed by dual-energy x-ray absorptiometry (DXA) (Norland Elite; Norland at Swissray, Fort Atkinson, WI).

2.2. High-resolution peripheral quantitative computed tomography (HRpQCT)

The non-dominant arm and contralateral leg were imaged using an HRpQCT scanner (XtremeCT II; Scanco Medical, Bruttisellen, Switzerland). Phantoms were imaged daily to confirm scanner stability. Bone length was measured in triplicate using a segmometer (Realmet Flexible Segmometer, NutriActiva, Minneapolis, MN) and as described by Bonaretti et al. (Bonaretti et al., 2017). Per convention, ulna length (mm) was measured as a surrogate for radial length. The skin overlying the distal apex of the ulnar styloid was marked and the elbow placed on a rigid surface. The Euclidean distance between the surface and styloid mark was measured. Tibial length (mm) was measured between skin marks placed at the distal tip of the medial malleolus and medial knee joint line. Short-term precision for repeat mark placement and length measures of the ulna and tibia in 15 individuals tested on two consecutive days showed root mean square standard deviations of 2.8 mm (1.1 %) and 6.3 mm (1.7 %), respectively.

Scans were acquired and reconstructed as previously described (Warden et al., 2021a). Subjects laid supine with their limb immobilized using an anatomically formed carbon fiber cast. The scanner operated at 68 kVp and 1.47 mA to acquire 168 slices (10.2 mm of bone length) with a voxel size of 60.7 μm. After performance of a scout view, reference lines were placed at the medial edge of the distal radius articular surface and center of the distal tibia joint surface. Scan stacks were centered 30 % of bone length proximal to the reference lines. The 30 % location was chosen as it is accessible in most individuals when using the manufacturer's standard forearm and leg casts on a second generation HRpQCT scanner. Assessment of more proximal sites requires use of custom casts and different reference line landmarks to stay within the z-axis limits of the scanner. Scans were scored for motion artifacts on a standard scale of 1 (no motion) to 5 (discontinuities in the cortical shell) (Sode et al., 2011). Scans scoring ≥3 were repeated when time permitted. Scans with a motion artifact of 4 or 5 were excluded from analyses.

A manufacturer provided evaluation script using a dual threshold technique was used to contour the outer periosteal surface and inner trabecular/medullary compartment. Manufacturer provided evaluation scripts were used to obtain outcomes (Table 1). A standard cortical bone script was used to obtain CtvBMD, CtAr, CtPm, CtTh, and CtPo. The script utilized a low-pass Gaussian filter (sigma 0.8, support 1.0 voxel) and fixed thresholds of 320 and 450 mgHA/cm^3 to extract trabecular and cortical bone, respectively. Only cortical outcomes were recorded as diaphyseal sites contain limited trabecular bone. The manufacturer's 'bone midshaft evaluation' script was used with a low-pass Gaussian filter (sigma 0.8, support 1.0) and outer threshold of 450 mgHA/cm^3. The evaluation provided outcomes for the whole bone (i.e. cortical and any trabecular bone) as the script was run with a single outer contour and without an inside clock-wise (i.e. 'negative' excluding) contour. Outcomes obtained were TotDen (identified as 'Mean1' in the manufacturer's script), TMD (identified as 'Mean2' in the manufacturer's script), TA, BA, BA/TA, I_{MIN}, I_{MAX}, and pMOI. Stiffness and failure load were estimated by μFE analysis (Scanco Medical FE software version 1.13). Each voxel within the segmented images was assigned a modulus of 10 GPa and Poisson's ratio of 0.3. Axial compression was applied and failure load estimated when 5 % of elements exceeded 1 % strain (Arias-

Table 1
HR-pQCT outcomes.

Outcome	Abbreviation	Units	Description
Total density ('Mean1')[b]	TotDen	mgHA/cm^3	Average density of all voxels within the periosteal contour, including tissue and voids (i.e. medullary cavity and pores)
Tissue mineral density ('Mean2')[b]	TMD	mgHA/cm^3	Average density of all voxels within the periosteal contour with a density >450 mgHA/cm^3 (excludes medullary cavity and pores)
Cortical vBMD[a]	CtvBMD	mgHA/cm^3	Average density of all voxels within the segmented cortical compartment (includes pores)
Total area[b]	TA	mm^2	Area within the periosteal contour, including tissue and voids (i.e. medullary cavity and pores)
Bone area[b]	BA	mm^2	Area within the periosteal contour with a density >450 mgHA/cm^3 (excludes medullary cavity and pores)
Cortical area[a]	CtAr	mm^2	Average cross-sectional area of the segmented cortical compartment (includes pores)
Bone area/total area[b]	BA/TA	%	Proportion of voxels within the periosteal contour with a density >450 mgHA/cm^3
Cortical perimeter[a]	CtPm	mm	Average length of the outer periosteal surface within the segmented cortical compartment
Cortical thickness[a]	CtTh	mm	Thickness of cortical bone including any pores
Cortical porosity[a]	CtPo	%	Percentage of void voxels from the total cortical voxels in the segmented cortical compartment
Minimum second moment of area[b]	I_{MIN}	mm^4	Estimated ability of all the components within the outer contour with a density >450 mg/cm^3 to resist bending on the direction of least bending resistance
Maximum second moment of area[b]	I_{MAX}	mm^4	Estimated ability of all the components within the outer contour with a density >450 mg/cm^3 to resist bending on the direction of most bending resistance
Polar moment of inertia[b]	pMOI	mm^4	Estimated ability of all the components within the outer contour with a density >450 mg/cm^3 to resist torsional loading
Stiffness[c]	–	kN/mm	Total reaction force divided by the applied displacement within the finite model
Failure load[c]	–	N	Failure load indirectly estimated from linear finite element model

[a] Acquired using the manufacturer's standard cortical bone script, a low-pass Gaussian filter (sigma 0.8, support 1.0 voxel) and fixed thresholds of 450 and 320 mgHA/cm^3 for cortical and trabecular bone, respectively.
[b] Acquired using the manufacturer's 'bone midshaft evaluation' script, a low-pass Gaussian filter (sigma 0.8, support 1.0 voxel) and fixed threshold of 450 mgHA/cm^3.
[c] Acquired using the manufacturer's μFE analysis with voxels assigned a modulus of 10 GPa and Poisson's ratio of 0.3. Failure estimated when 5 % of elements exceeded 1 % strain.

Moreno et al., 2019).

2.3. Statistical analyses

All statistical analyses were performed for females and males separately as skeletal proportions and cross-sectional properties differ across sexes independent of height and weight (Kun et al., 2023; Nieves et al., 2005). Participant characteristics were described according to decade stage of life (18–29, 30–39, 40–49, 50–59, 60–69, and 70+ yrs). Spearman partial correlation controlling for age was used to assess the relationship between HRpQCT outcomes and bone length.

Scaling factors were calculated for HRpQCT outcomes exhibiting a Spearman partial correlation (on age) with bone length of $R^2 \geq 0.05$. Scaling factors were calculated using the simple allometric linear regression model, $Y = \alpha X^{\beta}\varepsilon$, applied in natural logarithmic form as:

$$log_e Y = log_e \alpha + \beta\, log_e X + log_e \varepsilon$$

with Y the HRpQCT outcome of interest, X the predictor variable (i.e., bone length), β the scaling exponent or power (scaling factor), α the proportionality constant, and ε the multiplicative error. HRpQCT outcomes exhibiting a Spearman partial correlation with bone length of $R^2 < 0.05$ (i.e., <5 % of the variation explained) were considered to have low explanatory value.

Scaling factors were used to scale HRpQCT outcomes as:

$$Y_{scaled} = Y_{raw} / (X/X_0)^{SF}$$

with Y_{scaled} the scaled value for the HRpQCT outcome, Y_{raw} the original measured value for the HRpQCT outcome, X the bone length, X_0 the sex-specific median bone length within the study population, and SF the scaling factor (β) from the linear regression model. Bone length (X) was normalized to sex-specific median bone length (X_0) so that the scaled value retained the same units and were in a similar value range as the original measured value for the HRpQCT outcome.

Sex-specific reference centile curves for raw and scaled HRpQCT outcomes were generated using the LMS method (Cole and Green, 1992) with R package GAMLSS (version 5.2.0) (Rigby and Stasinopoulos, 2005). The LMS method uses Box-Cox transformation to achieve normality at a given age (Box-Cox Cole and Green [BCCG] distribution). Nonparametric smooth curves are fit to the parameter values across the age range using penalized likelihood with penalty on the second derivatives.

Centile curves and z-scores were calculated from the estimated parameter curves. LMS-derived z-scores are not suited for identifying extreme values because the LMS transformation method to achieve normality constrains maximum obtainable z-scores. Modified z-scores are provided for scores greater than +2 to address this. In modified z-scores, the HRpQCT outcome is expressed relative to the sex- and age-matched median in units of half the distance between 0 and + 2 z-scores, as per the approach used for growth charts (Centers for Disease Control and Prevention, n.d.).

3. Results

3.1. Participant and scan characteristics

Scans from 1426 participants (1034 females, 392 males) were included following exclusion of 430 participants due to: 1) race not White (n = 247, including 87 with a self-reported ineligible disease) and 2) race White, but self-reported ineligible disease or illness (n = 183). The final cohort included females and males ranging in age from 18.0 to 85.3 yrs. and 18.4 to 83.6 yrs., respectively. Participant characteristics stratified by decade of age are detailed in Table 2. Total hip and/or spine aBMD t-score was −1 to −2.5 and ≤−2.5 in 336 (32.5 %) and 20 (1.9 %) females, respectively. One hundred fifty (38.3 %) and 21 (5.4 %) males had a total hip and/or spine aBMD t-score −1 to −2.5 and <−2.5, respectively.

HRpQCT reference data in females was generated from 1023 and 919 scans of the radius and tibia, respectively (Table 2). Lower scan numbers than participants was due to: 1) scan not performed due to time constraints (n = 5 radius and 59 tibia scans); 2) excessive motion artifact (n = 26 radius and 9 tibia scans), and; 3) participant size (e.g. leg too large for the carbon fiber cast; leg too long to place the reference line and scan

Table 2
Participant characteristics stratified by decade of age[a].

Characteristic	Age group (yrs)					
	18–29	30–39	40–49	50–59	60–69	70+
Females						
n	184	113	126	224	286	101
Height (m)	1.66 (1.61–1.70)	1.66 (1.62–1.70)	1.64 (1.61–1.68)	1.63 (1.60–1.67)	1.63 (1.59–1.67)	1.62 (1.58–1.65)
Ulna length (cm)	25.5 (24.4–26.4)	25.4 (24.6–26.2)	25.3 (24.5–26.1)	25.3 (24.4–26.3)	25.2 (24.3–26.0)	25.3 (24.6–25.9)
Tibia length (cm)	37.0 (35.4–38.3)	36.9 (35.7–37.9)	36.5 (34.8–38.0)	36.7 (35.1–37.9)	36.7 (35.2–38.1)	36.5 (35.1–37.9)
Weight (kg)	71.5 (59.0–76.8)	71.4 (60.0–79.6)	74.1 (60.4–87.1)	74.1 (60.6–83.6)	73.5 (62.3–82.5)	69.3 (59.4–76.9)
BMI (kg/m^2)	25.9 (21.7–27.7)	25.9 (21.6–29.5)	27.6 (21.9–33.0)	27.7 (22.8–31.5)	27.8 (23.2–31.1)	26.5 (22.7–29.3)
Physical function						
Grip strength (kg)	27.9 (23.5–32.0)	29.5 (26.0–32.5)	26.8 (22.3–31.1)	25.3 (21.6–28.3)	23.9 (21.0–26.8)	21.8 (17.7–25.0)
5× sit-to-stand test (s)	8.6 (7.1–9.9)	8.7 (7.2–10.1)	9.0 (7.4–10.5)	9.3 (7.7–10.6)	10.3 (8.6–11.5)	10.9 (9.0–12.8)
PROMIS-PF (T-score)	58.0 (52.4–63.5)	57.1 (51.2–63.5)	54.7 (48.7–59.6)	52.5 (47.1–57.8)	50.5 (47.1–54.7)	48.6 (44.6–53.6)
Bone densitometry						
Spine aBMD z-score	0.37 (−0.32–0.95)	0.42 (−0.13–0.90)	0.32 (−0.53–1.13)	0.04 (−0.79–0.78)	0.39 (−0.52–1.23)	1.07 (0.42–1.85)
Total hip aBMD z-score	0.76 (0.06–1.51)	0.64 (0.06–1.24)	0.47 (−0.41–1.30)	0.27 (−0.57–0.94)	0.27 (−0.36–0.89)	0.66 (0.13–1.18)
HRpQCT scans included (*n*)						
Radial diaphysis	182	112	123	224	283	99
Tibial diaphysis	162	103	115	195	257	87
Males						
n	105	45	37	41	95	69
Height (m)	1.79 (1.74–1.83)	1.77 (1.74–1.81)	1.78 (1.73–1.84)	1.76 (1.72–1.83)	1.78 (1.74–1.81)	1.75 (1.70–1.79)
Ulna length (cm)	28.2 (27.1–28.8)	27.6 (26.8–28.7)	27.9 (26.7–29.0)	27.9 (27.0–28.9)	28.1 (26.9–29.2)	27.8 (26.9–28.9)
Tibia length (cm)	40.1 (39.0–41.5)	39.1 (38.0–40.7)	39.5 (37.7–41.0)	39.4 (37.8–41.2)	40.0 (38.3–41.3)	39.5 (37.6–40.7)
Weight (kg)	85.2 (73.9–91.6)	85.2 (75.1–93.0)	88.4 (79.3–95.8)	88.8 (76.9–100.3)	88.2 (76.1–97.2)	87.0 (75.8–95.8)
BMI (kg/m^2)	26.5 (23.5–28.6)	27.3 (24.6–30.7)	28.0 (24.7–30.8)	28.5 (24.4–31.4)	27.8 (24.2–30.4)	28.4 (25.1–31.4)
Physical function						
Grip strength (kg)	47.6 (40.7–55.5)	47.4 (40.4–54.9)	48.3 (43.0–53.2)	44.6 (42.0–48.6)	41.3 (32.9–48.1)	31.6 (24.8–39.2)
5× sit-to-stand test (s)	8.5 (7.0–9.6)	8.2 (6.1–9.6)	8.8 (7.3–9.4)	9.0 (7.3–9.9)	9.8 (7.9–11.1)	11.7 (8.9–13.2)
PROMIS-PF (T-score)	60.1 (55.8–64.7)	58.7 (53.1–66.2)	57.1 (50.5–64.5)	53.3 (47.7–60.6)	53.4 (49.2–57.3)	48.0 (45.2–51.6)
Bone densitometry						
Spine aBMD z-score	0.05 (−0.63–0.59)	−0.29 (−0.90–0.05)	−0.07 (−1.02–0.55)	0.06 (−0.58–0.72)	0.90 (0.01–1.66)	0.56 (−0.22–1.19)
Total hip aBMD z-score	0.04 (−0.86–0.80)	−0.28 (−1.1–0.25)	−0.12 (−0.80–0.49)	−0.09 (−0.81–0.52)	0.25 (−0.55–0.88)	−0.12 (−0.68–0.30)
HRpQCT scans included (*n*)						
Radial diaphysis	104	44	37	40	91	68
Tibial diaphysis	90	41	32	37	81	55

aBMD = areal bone mineral density; BMI = body mass index; HRpQCT = high-resolution peripheral quantitative computed tomography; PROMIS-PF = physical function domain of the National Institues of Health Patient-Reported Outcomes Measurement Information System.
[a] Data are median (interquartile range), except for frequencies.

stack within the constraints of the z-axis of the scanner; presence of a local tomography artifact due to absorbing tissue outside of field of view) (n = 47 tibia scans).

Reference data in males was generated from 384 and 336 scans of the radius and tibia, respectively (Table 2). Lower scan numbers than participants was due to: 1) scan not performed due to time constraints (n = 6 radius and 31 tibia scans); 2) excessive motion artifact (n = 2 radius and 1 tibia scans) and; 3) participant size (n = 24 tibia scans).

3.2. Correlations and scaling factors

There were negative relationships between density outcomes (TotDen, TMD, CtvBMD) and bone length at both the radius and tibia in females and males (all partial correlations = −0.191 to −0.055) (Table 3). However, correlations did not rise to the level of $R^2 \geq 0.05$ required for density data to be scaled to bone length. Similarly, bone length had low value in explaining radial and tibial BA/TA, CtTh or CtPo in either sex (all $R^2 < 0.05$).

Bone length explained 8.7 % to 13.6 % of the variance in radius areas (TA, BA, CtAr) and 9.9 % to 19.3 % of the variance in tibial areas (TA, BA, CtAr) in both sexes (Table 3). Areas in females scaled to length with scaling factors ranging from 0.934 to 1.009 for both the radius and tibia. Areas in males scaled to length with scaling factors ranging from 0.685 to 0.888 at the tibia and 0.856 to 0.984 at the radius.

There were positive relationships at both sites and in each sex between bone length and the estimated ability to resist bending (I_{MIN}, I_{MAX}), torsion (pMOI), and compression forces (stiffness and failure load) (all partial correlations = 0.280 to 0.452) (Table 3). Bone length explained 7.9 % to 20.5 % of the variance in the estimated mechanical properties. The highest scaling factors at both sites and in both sexes were for bone length's relationship with the estimated ability to resist bending (I_{MIN}, I_{MAX}) and torsion (pMOI) (all scaling factors = 1.652 to 2.113). Estimated ability to resist compression forces (stiffness and failure load) scaled to length at both the radius and tibia with scaling factors ranging from 0.934 to 1.019 in females and 0.685 to 0.984 in males.

3.3. Centile curves

Centile curves for raw CtvBMD, CtTh and CtPo outcomes, which did not satisfactorily scale to bone length, have previously been published (Warden et al., 2022b). Similar curves for TotDen, TMD, and BA/TA at the radius and tibia are presented in Supplemental Files 1 and 2, respectively. The fitted median centile curve for TMD peaked between 35 and 40 years of age in both sexes before declining thereafter. The decline in females was more precipitous, especially between 40 and 60 years of age.

HRpQCT raw values for outcomes correlating with bone length at $R^2 \geq 0.05$ (TA, BA, CtAr, CtPm, I_{MIN}, I_{MAX}, pMOI, stiffness, failure load) were converted to scaled values using the scaling factors and the ratio of the individual's bone length to sex specific median bone length (females = 25 cm for 'radius' and 37 cm for tibia; males = 28 cm for 'radius' and 40 cm for tibia). For example, for a female with a radial bone length of 24.2 cm and raw I_{MIN} outcome of 514 mm^4, the scaled I_{MIN} would be

Table 3
Spearman partial (on age) correlation between bone length and HRpQCT outcomes, and scaling factors (SF) for outcomes exhibiting correlation with an $R^2 > 0.05$.

Site and HRpQCT outcome	Female			Male		
	Spearman	R^2	SF	Spearman	R^2	SF
Radius						
TotDen	−0.067	0.004	–	−0.120	0.014	–
TMD	−0.109	0.012	–	−0.144	0.021	–
CtvBMD	−0.088	0.008	–	−0.145	0.021	–
TA	0.376	0.141	1.009	0.329	0.108	0.984
BA	0.369	0.136	0.934	0.303	0.092	0.866
CtAr	0.367	0.135	0.934	0.296	0.087	0.856
BA/TA	−0.048	0.002	–	−0.082	0.007	–
CtPm	0.356	0.127	0.503	0.329	0.108	0.530
CtTh	0.170	0.029	–	0.138	0.019	–
CtPo	−0.010	0.010	–	−0.008	<0.001	–
I_{MIN}	0.418	0.175	2.095	0.353	0.125	1.989
I_{MAX}	0.325	0.105	1.852	0.284	0.081	1.858
pMOI	0.371	0.138	1.951	0.320	0.103	1.912
Stiffness	0.370	0.137	0.966	0.291	0.085	0.865
Failure load	0.363	0.132	0.934	0.280	0.079	0.829
Tibia						
TotDen	−0.055	0.003	–	−0.218	0.048	–
TMD	−0.191	0.036	–	−0.209	0.044	–
CtvBMD	−0.182	0.033	–	−0.222	0.049	–
TA	0.439	0.193	0.999	0.419	0.176	0.888
BA	0.409	0.168	0.959	0.328	0.107	0.702
CtAr	0.406	0.165	0.949	0.314	0.099	0.685
BA/TA	−0.002	0.000	–	−0.147	0.022	–
CtPm	0.444	0.197	0.544	0.172	0.415	0.508
CtTh	0.207	0.043	–	0.070	0.005	–
CtPo	0.027	<0.001	–	0.159	0.025	–
I_{MIN}	0.393	0.154	1.831	0.374	0.140	1.652
I_{MAX}	0.443	0.196	2.113	0.397	0.158	1.755
pMOI	0.452	0.205	2.009	0.418	0.175	1.713
Stiffness	0.424	0.179	1.007	0.318	0.101	0.700
Failure load	0.432	0.187	1.019	0.328	0.107	0.719

$514.5/(24.2/25)^{2.095} = 550.7$ mm^4.

Centile curves fitted to scaled TA, BA, pMOI, and failure load outcomes are presented for the radius (Fig. 1) and tibia (Fig. 2). Centile curves fitted to scaled CtAr, CtPm, I_{MIN}, I_{MAX}, and stiffness outcomes are provided in Supplemental Files 3 (radius) and 4 (tibia).

3.4. Percentile and z-score calculator, and centile curve plotter

Excel-based calculators were developed for both the radius (Supplemental File 5) and tibia (Supplemental File 6). Entry of basic demographic information (sex, date of birth, scan date, and bone length) and one or more HRpQCT outcome (Fig. 3A) results in plotting of sex-specific centile curves (Fig. 3B). The centile curves are based on the curves fitted using the LMS approach fitted to raw data (TotDen, TMD, CtvBMD, Ct.Th) or bone-length scaled data (TA, BA, CtAr, CtPm, I_{MIN}, I_{MAX}, pMOI, stiffness, failure load), depending on whether the outcome was related to bone length at $R^2 \geq 0.05$. Beneath each curve, the raw entered and bone length scaled value for the HRpQCT outcome is provided along with the associated z-score and percentile (Fig. 3C). The raw z-score and percentile are derived from curves fitted to the raw reference data, whereas the scaled z-score and percentile are derived from curves fitted to the scaled reference data.

4. Discussion

The current study expands our previously published reference data for HRpQCT outcomes at the cortical bone rich radial and tibial diaphyses (Warden et al., 2022b). We included data in the current analyses from an additional 173 radius (+20 %) and 171 tibia (+23 %) scans in females and an additional 82 radius (+27 %) and 88 (+35 %) tibia scans in males. Beyond an expanded dataset, the current study provides centile curves for HRpQCT outcomes previously without reference data, including TotDen, TMD, TA, BA, BA/TA, I_{MIN}, I_{MAX}, and pMOI. In addition, we explored the relationship between bone length and HRpQCT outcomes, developed a means of scaling outcomes for bone length, and generated centile curves for bone length adjusted outcomes. To facilitate the utility of the latter curves, Excel-based calculators (Supplementary Files 5 and 6) were developed to calculate age- and sex-matched percentiles and z-scores for both raw and bone length adjusted outcomes.

Many of the HRpQCT outcomes at the radial and tibial diaphysis in both sexes were related to bone length, consistent with established interrelationships between bone length and cross-sectional size (Biewener, 2005; Ruff, 1984). Size outcomes (TA, BA, CtAr, CtPm) positively correlated with bone length confirming that individuals with longer bones also had wider bones. As bones with larger cross-sectional size have material distributed further from bending axes, bone length also correlated with estimates of bone rigidity and strength (I_{MIN}, I_{MAX}, pMOI, stiffness, failure load). There were no relationships between bone length and TotDen, TMD, CtvBMD, and BA/TA as the later HRpQCT outcomes are already expressed relative to bone size.

There was no relationship between CtTh and bone length. This is consistent with previous work (Bjørnerem et al., 2013) and likely reflects a means of minimizing the energy costs of larger and heavier bones. Bending resistance increases to the fourth power of the radius of a bone. By placing material further from its central axis and increasing its radius, a larger bone is disproportionately stronger for the same mass and energy cost. The more distant distribution of material relatively thins the cortex such that CtTh does not correspondingly increase with the increase in size of longer bones. Despite the relatively thinner CtTh, compressive strength is preserved via the increase in CtAr as bone length increases (Seeman, 2003).

Scaling factors were calculated for outcomes for which bone length explained at least 5 % of variance (i.e., $R^2 \geq 0.05$). There is no accepted cut-off in the literature. Our cut-off was chosen based on the rationale that a lesser relationship implied bone length had limited explanatory value, and is a more liberal cut-off than (for example) the 10 % cut-off implemented when adjusting DXA Z-scores for height in children (Zemel et al., 2011). Outcomes expressed in linear dimensions (e.g., CtPm) exhibited negative allometry, with scaling factors around 0.5 indicating disproportionately lower increases in size relative to increases in bone length. Relatively isometric allometry (scaling factors around one) was observed for outcomes expressed in squared linear dimensions (e.g., TA, BA, CtAr), indicating bone cross-sectional area measures increased proportionally as bone length increased. Outcomes to the fourth power of linear dimensions (e.g., I_{MIN}, I_{MAX}, pMOI) exhibited positive allometry with scaling factors around two. The latter indicates estimated bone rigidity had disproportionately greater increases relative to increases in bone length.

The scaling factors were used to scale HRpQCT outcomes to bone length, and centile curves were generated for both raw and bone length scaled HRpQCT data. The centile curves can be used to calculate z-scores. Excel-based calculators are provided to facilitate this process (Supplementary Files 5 and 6). The raw and scaled z-scores indicate the magnitude that an individual's HRpQCT outcomes differ relative to expected sex- and age-specific values. The difference between the two z-scores being that the scaled z-score also considers bone length.

The consideration of bone length enables it to be determined whether an individual has normal sized bones for their bone length. For example, consider a 43-year-old female with a tibial length of 33.5 cm and tibial pMOI of 15,000 mm^4. Their raw z-score for pMOI using the Excel-based calculator equates to −0.738 indicating they have lower than expected torsional rigidity for their sex and age. This may be suggestive of reduced cross-sectional bone development and an increased risk of injury, such as a bone stress injury (Warden et al., 2021b).

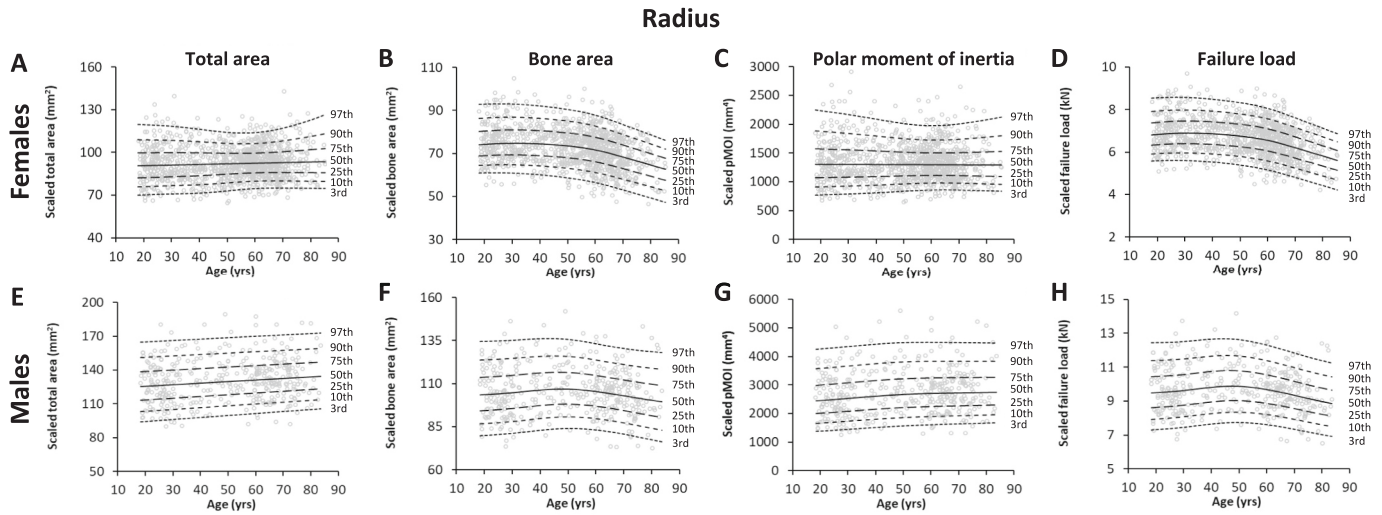

Fig. 1. Bone length scaled data and fitted centile curves for total area (A, E), bone area (B, F), polar moment of inertia (C, G), and estimated failure load (D, H) at the radial diaphysis for females (top row) and males (bottom row).

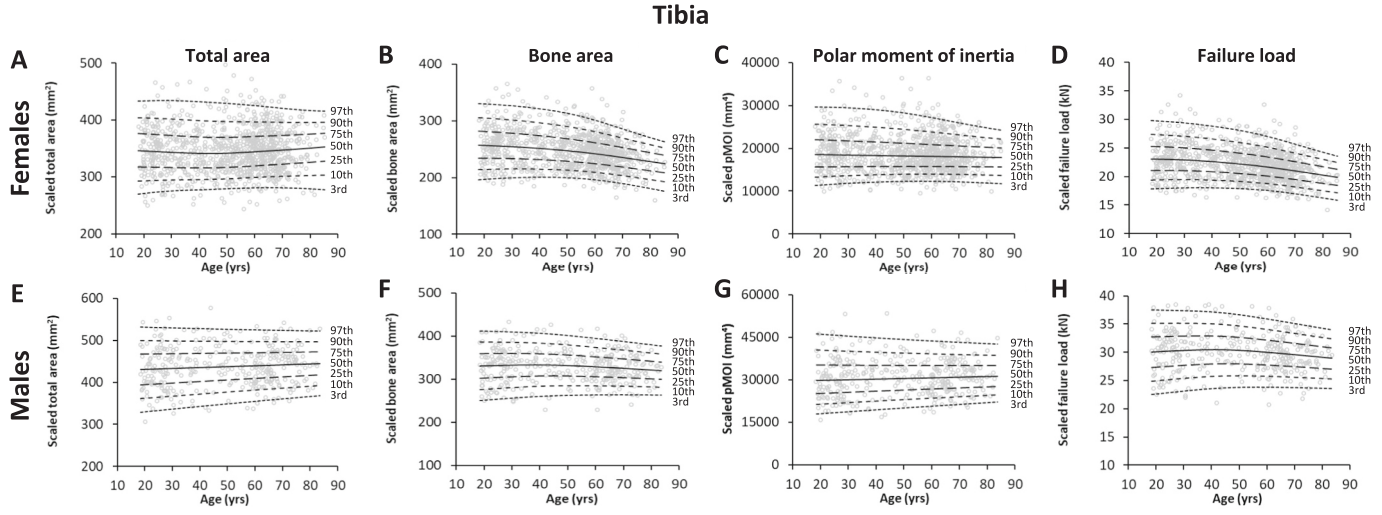

Fig. 2. Bone length scaled data and fitted centile curves for total area (A, E), bone area (B, F), polar moment of inertia (C, G), and estimated failure load (D,H) at the tibial diaphysis for females (top row) and males (bottom row).

However, the individual also has a tibial length that is lower than the median 37 cm for females. When bone length is considered, a scaled pMOI of 18,314 mm^4 is calculated ($15{,}000/[33.5/37]^{2.009}$) and a scaled z-score of −0.002 obtained indicating relatively normal torsional rigidity for their bone length.

Scaled HRpQCT outcomes will be higher and lower than raw HRpQCT outcomes for individuals with bone lengths shorter and longer than median values in the current reference cohort, respectively. This is because scaled values were normalized to sex-specific median bone length. The latter was performed so that scaled outcomes would retain the same units and be within the same range as raw outcomes. However, the scaling approach in our cohort does raise the question of whether the bone lengths in our cohort are representative.

Percutaneous measures of ulna (used as a surrogate for radius length) and tibia length are increasingly being performed prior to HRpQCT to enable the scanning region to be positioned relative to bone length, which has advantages over scanning at a fixed distance offset (Bonaretti et al., 2017; Ghasem-Zadeh et al., 2017; Okazaki et al., 2021; Shanbhogue et al., 2015). However, measured mean or median bone lengths are either not reported (Shanbhogue et al., 2015), not dichotomized by sex (Bonaretti et al., 2017; Shanbhogue et al., 2015) or acquired in a race and/or ethnicity with a different stature (Okazaki et al., 2021), negating the ability to compare to lengths acquired in the current study. Ghasem-Zadeh et al. (Ghasem-Zadeh et al., 2017) did report forearm lengths in White females (25.7 cm) and males (28.1 cm) which compare favorably to our measured lengths of 25 cm and 28 cm in females and males, respectively. Similarly, comparable lengths of 24.7 cm and 27.5 cm have been reported in another cohort of White females and males, respectively (Madden et al., 2012), and the 40 cm tibial length in males in our study matches the 40.2 cm measured in 18-year-old U.S. military recruits (Nieves et al., 2005).

In the absence of a wealth of percutaneously measured bone length data in the literature, a feasible proxy is to compare the heights of our individuals to population norms. Height and bone length are closely related, so much so that bone length is frequently used to estimate an individual's height. The average height within each decade of age in our cohort (Table 2; females = 1.62–1.64 m, males = 1.75–1.79 m) matches that of the U.S. White adult population (females = 1.62 m, males = 1.77 cm) (Fryar et al., 2021). The comparable height provides confidence that our measured median bone lengths are representative of the broader U.S. White population.

We assessed other outcomes to explore the comparability of our

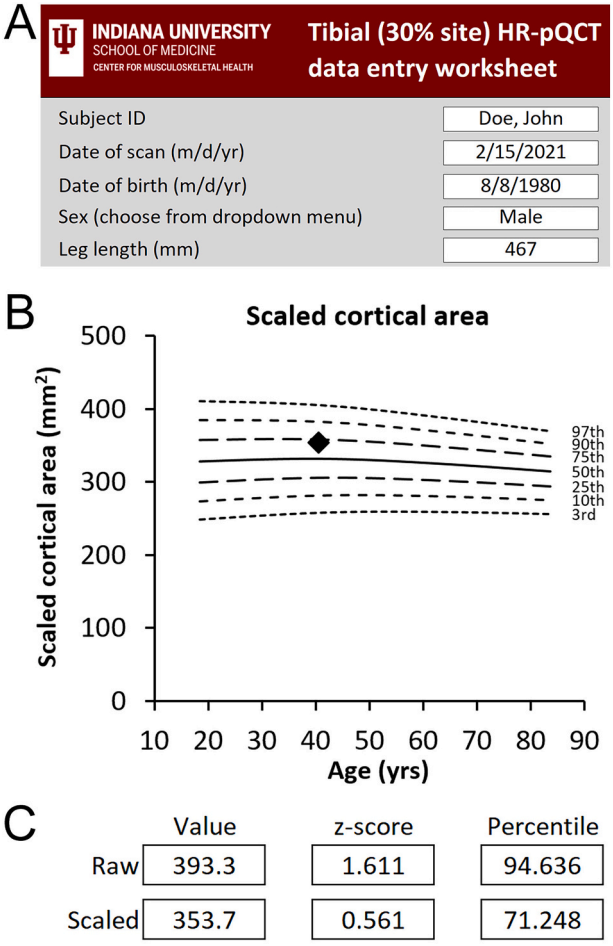

Fig. 3. Screenshots of the Excel-based calculator for tibia outcomes (available in Supplemental File 5). Following entry of basic demographic information and one or more HRpQCT outcome (A), centile curves are plotted (B), and sex- and age-specific raw and bone length scaled z-scores and percentiles are calculated (C).

cohort to the broader population, including DXA-derived bone outcomes, performance on physical function tests, and self-reported physical function (Table 1). DXA z-scores at the hip and spine were slightly higher than zero in females and approximated zero in males. Grip strength in our cohort according to decade stage of life mirrored reference values for individuals residing in the U.S. (Wang et al., 2018), whereas time to complete five sit-to-stand maneuvers matched or was slightly slower (Bohannon, 2006; Bohannon et al., 2010). Self-reported physical function (PROMIS-PF T-score) was slightly above the population mean of 50, depending on sex and decade stage of life. These cumulative data suggest our cohort had slightly above-to-normal general bone health and equivalent or a slightly higher level of functioning than the general U.S. population.

Our study has several strengths, but it is also not without limitations. Data were obtained at a single center and variability in machine performance at other centers may influence outcomes. The outcomes are specific to the sites scanned and the scanning, segmentation, and analysis procedures used. We used the manufacturer's 'bone midshaft evaluation' script with a single outer contour and without an inner clockwise (i.e., 'negative' excluding) contour. This means that outcomes using this script (including TotDen and TMD) include any trabecular bone present at the scan sites. This approach was selected as we wanted to include any trabecularized cortical bone, which increases with age (Zebaze et al., 2010). The micro-finite element model used to estimate bone strength is specific to axial compressive loading and was principally developed for distal bone sites with a greater proportion of trabecular bone. The ability of the model to estimate failure load in other loading directions and at the cortical bone rich diaphysis remains to be established. Finally, we had more limited inclusion of males and older (age >70 yrs) adults and our data are specific to White individuals living in the Midwest of the United States. HRpQCT outcomes vary by race potentially requiring the generation of separate reference data for other races (van den Bergh et al., 2021).

In summary, the current study expands our previous dataset by providing reference data for additional HRpQCT outcomes, including TotDen, TMD, TA, BA, BA/TA, I_{MIN}, I_{MAX}, and pMOI. More importantly, the study provides a means of scaling outcomes for bone length and provides reference data for bone length adjusted outcomes. The reference data enable HRpQCT outcomes in an individual (or population of interest) to be expressed relative to the reference cohort to determine if they are 'big boned' for their age, sex and bone length.

Supplementary data to this article can be found online at https://doi.org/10.1016/j.bonr.2024.101735.

CRediT authorship contribution statement

Stuart J. Warden: Conceptualization, Data curation, Formal analysis, Funding acquisition, Investigation, Methodology, Project administration, Supervision, Writing – original draft, Writing – review & editing. **Robyn K. Fuchs:** Conceptualization, Data curation, Formal analysis, Writing – review & editing. **Ziyue Liu:** Formal analysis, Writing – review & editing. **Katelynn R. Toloday:** Investigation, Writing – review & editing. **Rachel Surowiec:** Data curation, Investigation, Methodology, Writing – review & editing. **Sharon M. Moe:** Conceptualization, Funding acquisition, Supervision, Writing – review & editing.

Declaration of competing interest

None.

Data availability

Data will be made available on request.

Acknowledgements

This contribution was made possible by support from the National Institutes of Health (NIH/NIAMS P30 AR072581), and the Indiana Clinical Translational Science Award/Institute (NCATS UL1TR002529-01).

References

Arias-Moreno, A.J., Hosseini, H.S., Bevers, M., Ito, K., Zysset, P., van Rietbergen, B., 2019. Validation of distal radius failure load predictions by homogenized- and micro-finite element analyses based on second-generation high-resolution peripheral quantitative CT images. Osteoporos. Int. 30 (7), 1433–1443. https://doi.org/10.1007/s00198-019-04935-6.

Biewener, A.A., 2005. Biomechanical consequences of scaling. J. Exp. Biol. 208 (9), 1665–1676. https://doi.org/10.1242/jeb.01520.

Bjørnerem, Å., Bui, Q.M., Ghasem-Zadeh, A., Hopper, J.L., Zebaze, R., Seeman, E., 2013. Fracture risk and height: an association partly accounted for by cortical porosity of relatively thinner cortices. J. Bone Miner. Res. 28 (9), 2017–2026. https://doi.org/10.1002/jbmr.1934.

Bohannon, R.W., 2006. Reference values for the five-repetition sit-to-stand test: a descriptive meta-analysis of data from elders. Percept. Mot. Skills 103 (1), 215–222. https://doi.org/10.2466/pms.103.1.215-222.

Bohannon, R.W., Bubela, D.J., Magasi, S.R., Wang, Y.-C., Gershon, R.C., 2010. Sit-to-stand test: performance and determinants across the age-span. Isokinet. Exerc. Sci. 18, 235–240. https://doi.org/10.3233/IES-2010-0389.

Bonaretti, S., Majumdar, S., Lang, T.F., Khosla, S., Burghardt, A.J., 2017. The comparability of HR-pQCT bone measurements is improved by scanning anatomically standardized regions. Osteoporos. Int. 28 (7), 2115–2128. https://doi.org/10.1007/s00198-017-4010-7.

Cella, D., Yount, S., Rothrock, N., Gershon, R., Cook, K., Reeve, B., et al., 2007. The Patient-Reported Outcomes Measurement Information System (PROMIS): progress of an NIH Roadmap cooperative group during its first two years. Med. Care 45 (5 Suppl 1), S3–s11. https://doi.org/10.1097/01.mlr.0000258615.42478.55.

Centers for Disease Control and Prevention. Modified z-scores in the CDC growth charts. https://www.cdc.gov/nccdphp/dnpa/growthcharts/resources/biv-cutoffs.pdf. (Accessed 9 October 2023).

Cheung, A.M., Majumdar, S., Brixen, K., Chapurlat, R., Fuerst, T., Engelke, K., et al., 2014. Effects of odanacatib on the radius and tibia of postmenopausal women: improvements in bone geometry, microarchitecture, and estimated bone strength. J. Bone Miner. Res. 29 (8), 1786–1794. https://doi.org/10.1002/jbmr.2194.

Cole, T.J., Green, P.J., 1992. Smoothing reference centile curves: the LMS method and penalized likelihood. Stat. Med. 11 (10), 1305–1319. https://doi.org/10.1002/sim.4780111005.

Fryar, C.D., Carroll, M.D., Gu, Q., Afful, J., Ogden, C.L., 2021. Anthropometric reference data for children and adults: United States, 2015–2018. Vital Health Stat. 3 (36), 1–44.

Fuchs, R.K., Thompson, W.R., Warden, S.J., 2019. Bone biology. In: Pawelec, K.M., Planell, J.A. (Eds.), Bone Repair Biomaterials, 2nd ed. Woodhead Publishing, pp. 15–52.

Galilei, G., 1638. Dialogues Concerning Two New Sciences (Translated by H. Crew and A. De Salvio). Macmillan, New York.

Ghasem-Zadeh, A., Burghardt, A., Wang, X.F., Iuliano, S., Bonaretti, S., Bui, M., et al., 2017. Quantifying sex, race, and age specific differences in bone microstructure requires measurement of anatomically equivalent regions. Bone 101, 206–213. https://doi.org/10.1016/j.bone.2017.05.010.

Hughes, J.M., Gaffney-Stomberg, E., Guerriere, K.I., Taylor, K.M., Popp, K.L., Xu, C., et al., 2018. Changes in tibial bone microarchitecture in female recruits in response to 8 weeks of U.S. Army Basic Combat Training. Bone 113, 9–16. https://doi.org/10.1016/j.bone.2018.04.021.

Kazakia, G.J., Tjong, W., Nirody, J.A., Burghardt, A.J., Carballido-Gamio, J., Patsch, J. M., et al., 2014. The influence of disuse on bone microstructure and mechanics assessed by HR-pQCT. Bone 63, 132–140. https://doi.org/10.1016/j.bone.2014.02.014.

Kun, E., Javan, E.M., Smith, O., Gulamali, F., de la Fuente, J., Flynn, B.I., et al., 2023. The genetic architecture and evolution of the human skeletal form. Science 381 (6655), eadf8009. https://doi.org/10.1126/science.adf8009.

Lespessailles, E., Hambli, R., Ferrari, S., 2016. Osteoporosis drug effects on cortical and trabecular bone microstructure: a review of HR-pQCT analyses. Bonekey Rep. 5, 836. https://doi.org/10.1038/bonekey.2016.59.

Madden, A.M., Tsikoura, T., Stott, D.J., 2012. The estimation of body height from ulna length in healthy adults from different ethnic groups. J. Hum. Nutr. Diet. 25 (2), 121–128. https://doi.org/10.1111/j.1365-277X.2011.01217.x.

Mikolajewicz, N., Bishop, N., Burghardt, A.J., Folkestad, L., Hall, A., Kozloff, K.M., et al., 2020. HR-pQCT measures of bone microarchitecture predict fracture: systematic review and meta-analysis. J. Bone Miner. Res. 35 (3), 446–459. https://doi.org/10.1002/jbmr.3901.

Nieves, J.W., Formica, C., Ruffing, J., Zion, M., Garrett, P., Lindsay, R., et al., 2005. Males have larger skeletal size and bone mass than females, despite comparable body size. J. Bone Miner. Res. 20 (3), 529–535. https://doi.org/10.1359/JBMR.041005.

Okazaki, N., Chiba, K., Burghardt, A.J., Kondo, C., Doi, M., Yokota, K., et al., 2021. Differences in bone mineral density and morphometry measurements by fixed versus relative offset methods in high-resolution peripheral quantitative computed tomography. Bone 149, 115973. https://doi.org/10.1016/j.bone.2021.115973.

O'Leary, T.J., Wardle, S.L., Gifford, R.M., Double, R.L., Reynolds, R.M., Woods, D.R., et al., 2021. Tibial macrostructure and microarchitecture adaptations in women during 44 weeks of arduous military training. J. Bone Miner. Res. 36 (7), 1300–1315. https://doi.org/10.1002/jbmr.4290.

Orwoll, E.S., Blackwell, T., Cummings, S.R., Cauley, J.A., Lane, N.E., Hoffman, A.R., et al., 2022. CT muscle density, D3Cr muscle mass, and body fat associations with physical performance, mobility outcomes, and mortality risk in older men. J. Gerontol. A Biol. Sci. Med. Sci. 77 (4), 790–799. https://doi.org/10.1093/gerona/glab266.

Patsch, J.M., Burghardt, A.J., Yap, S.P., Baum, T., Schwartz, A.V., Joseph, G.B., et al., 2013. Increased cortical porosity in type 2 diabetic postmenopausal women with fragility fractures. J. Bone Miner. Res. 28 (2), 313–324. https://doi.org/10.1002/jbmr.1763.

Rigby, R.A., Stasinopoulos, D.M., 2005. Generalized additive models for location, scale and shape. J. R. Stat. Soc.: Ser. C: Appl. Stat. 54 (3), 507–554. https://doi.org/10.1111/j.1467-9876.2005.00510.x.

Ruff, C.B., 1984. Allometry between length and cross-sectional dimensions of the femur and tibia in *Homo sapiens* sapiens. Am. J. Phys. Anthropol. 65 (4), 347–358. https://doi.org/10.1002/ajpa.1330650403.

Samelson, E.J., Broe, K.E., Xu, H., Yang, L., Boyd, S., Biver, E., et al., 2019. Cortical and trabecular bone microarchitecture as an independent predictor of incident fracture risk in older women and men in the Bone Microarchitecture International Consortium (BoMIC): a prospective study. Lancet Diabetes Endocrinol. 7 (1), 34–43. https://doi.org/10.1016/s2213-8587(18)30308-5.

Seeman, E., 2003. The structural and biomechanical basis of the gain and loss of bone strength in women and men. Endocrinol. Metab. Clin. N. Am. 32 (1), 25–38. https://doi.org/10.1016/s0889-8529(02)00078-6.

Shanbhogue, V.V., Hansen, S., Halekoh, U., Brixen, K., 2015. Use of relative vs fixed offset distance to define region of interest at the distal radius and tibia in high-resolution peripheral quantitative computed tomography. J. Clin. Densitom. 18 (2), 217–225. https://doi.org/10.1016/j.jocd.2014.12.002.

Sode, M., Burghardt, A.J., Pialat, J.B., Link, T.M., Majumdar, S., 2011. Quantitative characterization of subject motion in HR-pQCT images of the distal radius and tibia. Bone 48 (6), 1291–1297. https://doi.org/10.1016/j.bone.2011.03.755.

van den Bergh, J.P., Szulc, P., Cheung, A.M., Bouxsein, M., Engelke, K., Chapurlat, R., 2021. The clinical application of high-resolution peripheral computed tomography (HR-pQCT) in adults: state of the art and future directions. Osteoporos. Int. https://doi.org/10.1007/s00198-021-05999-z.

Wang, Y.-C., Bohannon, R.W., Li, X., Sindhu, B., Kapellusch, J., 2018. Hand-grip strength: normative reference values and equations for individuals 18 to 85 years of age residing in the United States. J. Orthop. Sports Phys. Ther. 48 (9), 685–693. https://doi.org/10.2519/jospt.2018.7851.

Warden, S.J., Wright, C.S., Fuchs, R.K., 2021a. Bone microarchitecture and strength adaptation to physical activity: a within-subject controlled, HRpQCT study. Med. Sci. Sports Exerc. 53 (6), 1179–1187. https://doi.org/10.1249/MSS.0000000000002571.

Warden, S.J., Edwards, W.B., Willy, R.W., 2021b. Preventing bone stress injuries in runners with optimal workload. Curr. Osteoporos. Rep. 19 (3), 298–307. https://doi.org/10.1007/s11914-021-00666-y.

Warden, S.J., Sventeckis, A.M., Surowiec, R.K., Fuchs, R.K., 2022a. Enhanced bone size, microarchitecture, and strength in female runners with a history of playing multidirectional sports. Med. Sci. Sports Exerc. 54 (12), 2020–2030. https://doi.org/10.1249/mss.0000000000003016.

Warden, S.J., Liu, Z., Fuchs, R.K., van Rietbergen, B., Moe, S.M., 2022b. Reference data and calculators for second-generation HR-pQCT measures of the radius and tibia at anatomically standardized regions in White adults. Osteoporos. Int. 33 (4), 791–806. https://doi.org/10.1007/s00198-021-06164-2.

Warden, S.J., Liu, Z., Moe, S.M., 2022c. Sex- and age-specific centile curves and downloadable calculator for clinical muscle strength tests to identify probable sarcopenia. Phys. Ther. 102 (3), pzab299 https://doi.org/10.1093/ptj/pzab299.

Whittier, D.E., Boyd, S.K., Burghardt, A.J., Paccou, J., Ghasem-Zadeh, A., Chapurlat, R., et al., 2020. Guidelines for the assessment of bone density and microarchitecture in vivo using high-resolution peripheral quantitative computed tomography. Osteoporos. Int. 31 (9), 1607–1627. https://doi.org/10.1007/s00198-020-05438-5.

Zebaze, R.M.D., Ghasem-Zadeh, A., Bohte, A., Iuliano-Burns, S., Mirams, M., Price, R.I., et al., 2010. Intracortical remodelling and porosity in the distal radius and post-mortem femurs of women: a cross-sectional study. Lancet 375 (9727), 1729–1736. https://doi.org/10.1016/S0140-6736(10)60320-0.

Zemel, B.S., Kalkwarf, H.J., Gilsanz, V., Lappe, J.M., Oberfield, S., Shepherd, J.A., et al., 2011. Revised reference curves for bone mineral content and areal bone mineral density according to age and sex for black and non-black children: results of the bone mineral density in childhood study. J. Clin. Endocrinol. Metab. 96 (10), 3160–3169. https://doi.org/10.1210/jc.2011-1111.